Supplementary information for

Multidecadal land water and groundwater drought evaluation in Peninsular India

Abhishek*, Tsuyoshi Kinouchi
School of Environment and Society, Tokyo Institute of Technology, Yokohama 226-8503, Japan
Email: abhishek.a.ab@m.titech.ac.jp*, abhishekiit95@gmail.com*, kinouchi.t.ab@m.titech.ac.jp

This supplementary material file includes (as per the order of appearance),

1. Increasing water scarcity in Peninsular India

With a global increase in drought frequency and severity, the drought assessment has become of paramount importance in India's temperate climate, which predominantly governs crop productivity [1–3]. Unsustainable extraction by anthropogenic activities in conjunction with the climate shift to warmer temperature has reduced groundwater availability and impaired its quality, making it vulnerable to projected climate change and population growth [4,5]. The water scarcity in India has recently been expanded to the agriculturally important Peninsular India, where overexploitation of groundwater (GW) and fluctuations in monsoon rainfall may further magnify the prevailing GW stress and impose subsequent food security risks [6]. Some of the river basins located in Peninsular India are moderate to severely non-resilient to the hydrological disturbances and have experienced seasonal to long-term water shortages [6]. However, droughts in India are mostly reported based on the percentile of rainfall and sometimes even by visual drying of the land surface [7], highlighting a need for quantitative and robust drought characterization based on integrated water storage deficits (WSD). Under these circumstances, understanding the basin-scale hydrological fluxes becomes vital for better monitoring and characterizing droughts and subsequent water resources management under the prevailing conditions. In the absence of a real-time integrated drought monitoring platform in India, timely and reliable identification and classification of the drought events are in urgent need.

Although India receives an annual rainfall of 1200 mm (highest amongst countries of comparable size) [8], due to the highly uneven distribution in spatial and temporal scales, about half of the country is either already affected or vulnerable to the water deficit conditions at various levels of water scarcity [9–11]. This water scarcity situation in India, and in the study basins in Peninsular India, is expected to worsen due to the combined impact of natural (climatic shifts to warmer temperatures) and anthropogenic factors (the high water demand from the growing population). Since most of the water demands in the basins are met by the groundwater withdrawals, which are highly dependent on the fluctuating monsoon precipitation, understanding various factors governing the groundwater availability in the region becomes of paramount importance. As per the assessment by the Central Groundwater Board, the ratio of groundwater consumption to recharge is over 100% (i.e., consumption>recharge) in some parts of North-West India, implying the unsustainable use of the GW in the region [12]. Moreover, out of 6584 GW assessment units, 1034 are already over-exploited, and 253 are critical, and another 681 are semi-critical [12], affecting 33% area of India already and making another 28% area vulnerable to the water deficit conditions at various levels of water scarcity [9–11]. Apart from the dependence of livelihood, variabilities of the prevailing groundwater resources limit crop production and hamper economic development in the region. Therefore, there is a clear need for the basin-wise assessment of the GW resources, which will further assist in efficiently dealing with the storage fluctuations and consequences resulting from the monsoon variabilities and lead to effective irrigation scheduling in the agriculture dominant study region.

Although there have been several studies focusing on the North-West Indian region [8,13–17], the Peninsular Indian region remains largely unexplored, with only a few recent studies those too concentrate only on a short period (e.g., for 2002-2017 [18], for 2002-2016 [19]). To the best of our

knowledge, no study has been carried out to assess the basin-scale integrated and segregated water storage dynamics, holistic drought characterization, and assessment of various drought indices focusing on groundwater beyond the GRACE period. Therefore, in the current study, for the first time, we investigate the water storage dynamics for a period of 35 years (1980-2014) and its implications on the intermittent in-situ groundwater observations in the three river basins in Peninsular India, which comprise a total of ~22% geographical area of the country.

2. Rationale of employing Land Water Storage based WSDI

The traditional approach of drought quantification solely depends on the limited accuracy of the ground-based hydro-meteorological data. In-situ data stations and their records suffer from many limitations, including inhomogeneous and inadequate distribution of monitoring network, data gaps, unavailability at the required spatiotemporal scale, associated high installation and maintenance cost, measurement limits within near-surface zones, and need for high human resources [20,21]. Furthermore, the drought characterization imposes a difficulty because it must take a multitude of dimensions, viz., drought magnitude, duration, type, frequency, and severity, into account [21]. Conventional methods for assessing drought severity include many subjective and objective information, including hydro-meteorological data and drought impact reports [22]. Additionally, the lack of a comprehensive universal definition and poor understanding of its precursors lead to drought classification in various categories. The most popular drought indices among a total of more than 150 and around 74 operational indices are the Standardized Runoff Index (SRI), Standardized Precipitation Index (SPI), and Palmer Drought Severity Index (PDSI) [21,23]. SRI, SPI, and PDSI are used to determine the seasonal loss in streamflow, monitor short- and long-term regional precipitation dynamics, and characterize agro-climatological droughts, respectively [22,24–26]. All of these physically-based drought indices rely solely upon the meteorological parameters surface or subsurface water storage components and do not consider a combined effect of all these parameters [21,27]. Moreover, there is no mechanism in all these indices to incorporate the variability in all water storage components, and hence, they lack in providing the integrated water storage deficit information over the target area.

Amid the inherent drawbacks of traditional drought indices, researchers have recently sought integrated drought indices based on remotely sensed water storage data [21,22]. Drought indices should represent the overall state of water resources, thus providing a comprehensive view of droughts for more practical, accurate, and viable management and decision-making. Satellite observations followed by the postprocessing techniques have proven quite useful for adequate drought characterization and monitoring on the required spatial and temporal scales in the past decades, especially after the launch of Gravity Recovery and Climate Experiment (GRACE) satellites [28]. Drought characterization based on the remotely sensed data of land water storage (LWS) outperforms the traditional methods because it represents the integrated deficits in surface water, soil moisture, and groundwater over the region of interest and thus depicts the real picture of bulk water dynamics [21,29]. Many integrated drought indices, primarily GRACE based, have been introduced and employed to assess the droughts globally, including the hydrological drought index (GHDI) [30] applied for the continental United States, total

storage deficit index (TSDI) for Northwestern China [29] and the Saskatchewan River Basin in Canada [31], terrestrial water storage (TWS) anomaly index (TWSI) [32] for the Haihe River Basin, China at various spatiotemporal scales. However, these studies depend on limited data sources covering a short duration equal to that of GRACE records, thus lacking a robust global framework for long-term drought characterization. This data brevity issue with the GRACE data limits our ability to get insights into the water resources dynamics far beyond the GRACE records. In this context, given the ability of the PCR-GLOBWB 2.0 model (taken as an example for demonstration purpose in our study) to simulate the various water storage components, we hypothesize that the model output can be used for a robust but straightforward basin-scale decadal drought assessment in terms of the water storage deficits and subsequent characterization of droughts (magnitude, duration, severity, and recovery time), beyond the GRACE satellite observations. Further, we compared the water storage deficit index (WSDI) with sc-PDSI and SPI12. Since the contribution of the surface water component to LWS is negligible in the study area, SRI was not included in the analysis. WSDI (whether PCR-GLOBWB based: modelled WSDI ($WSDI_m$) or GRACE based: $WSDI_g$) accounts for both the natural processes (rain, infiltration, evaporation, storage, etc.) as well as the anthropogenic activities (groundwater abstraction, supply, irrigation, etc.) in the terrestrial hydrologic system, and therefore provide holistic assessment of the bulk water storage dynamics in the region. Moreover, unlike $WSDI_m$, $WSDI_g$ is free from the impact of the uncertainties arising from the water balance models or from the hydrometeorological forcing. Segregation of the natural and anthropogenic components of variability in various water storage components is beyond the scope of this study, and should be considered in the future research. Lastly, to address the challenge for a real-time monitoring framework imposed by the irregular measurements of the groundwater in the region, we assessed the ability of the water storage deficit index (WSDI) to substitute the groundwater drought index (GWDI). We show that $WSDI_g$ can be used for quick monitoring of the groundwater in the region thus eliminating the need of any model simulation and dependence on the sporadic in-situ observations.

3. PC Raster Global Water Balance version 2 (PCR-GLOBWB 2.0) model

PCR-GLOBWB 2.0 model, which is a conceptual and process-based global (except Greenland and Antarctica) hydrology and water resources model (GHWRM) with a computational grid of 5 arcmins (0.1°×0.1°) and simulates the hydrological fluxes at a daily time step [33]. The model integrates human water use with the dynamic water balance between surface and subsurface water storage in two vertically stacked soil layers (soil zone depth of 1.5 meters) using the five-module setup, namely 'irrigation and water use module', 'meteorological forcing module', 'land surface module', 'groundwater module' and the 'surface water routing module' [33,34]. The model considers both upward (e.g., capillary rise) and downward (e.g., deep percolation) fluxes between atmosphere and various model layers [35]. At each time step, the model first calculates the water demands for irrigation, industry, domestic, and livestock based on temperature and socioeconomic developments (e.g., Gross Domestic Product, electricity production, etc.) based on FAOSTAT data, and then compare these demands to the actual availability of the water resources in the region and finally calculates the return flows per sector [34]. The standard land cover parameterization of the 'land surface module', which considers the spatiotemporal variability in the vegetation properties (e.g., crop factor, leaf area index,

LAI), and soil types and texture, was used [33,36]. Except for the precipitation (which was retrieved from the IMD), WATCH Forcing Data based on ERA-Interim reanalysis (WFDEI, temperature, shortwave downwelling, and longwave downwelling radiation) were used [37], similar to a previous study [38].

Due to the non-availability of continuous ground data for model calibration, similar to the previous studies [33,38–42], the model was not calibrated, and the standard parameterization settings were used. Since precipitation has been shown the most critical parameter in model output rather than the model parameters' uncertainties [43–45], we have used the high quality regional daily precipitation data (0.25°x0.25°) from the India Meteorological Department for the study duration (https://www.imdpune.gov.in/;[46]). A spin-up period of 50 years using the hydro-meteorological data of the year 1901-1950 (IMD precipitation data is available for 118 years, 1901 to 2018; https://www.imdpune.gov.in/) was used to enable the groundwater volumes to be in equilibrium with the study's current climatic settings. Daily outputs of individual water storage components for each grid cell were converted to the basin averaged monthly time series (for consistency in comparison with GRACE-based estimates of GWS: GWS_g) and summed to get the modeled land water storage ($LWS_m = SMS_m + SWS_m + GWS_m$). Although the modeled surface water storage (SWS_m) was used in calculating LWS_m, it is not explicitly analyzed in the study because of its negligible contribution to LWS_m and subsequent insignificant decadal trends compared to other components. The long-term mean of LWS_m from 04/2002 to 12/2014 (consistent with LWS_g baseline time) was subtracted from LWS_m time-series to get the monthly anomaly series of LWS_m (figure S2).

Please note that we do not endorse the PCR-GLOBWB model over other global hydrological and water resource models (GHWRMs) such as WGHM (WaterGAP Global Hydrology Model, which also includes coupling of human water use and reservoir management although with different mechanisms of water abstraction, groundwater availability, among others, compared to PCR-GLOBWB) [33,47–49], among others [50], which have also been used for analyzing the land water storage at various global [38] or regional scales [18]. We have just chosen one global model for demonstration purposes of how well we can understand the dynamics and variability of land storage and its constituent components beyond the GRACE time period and subsequently assess the capability of land water storage (whether LWS_g or LWS_m) to depict the near-real-time groundwater situation in the region.

Regarding the global hydrological model, it should be calibrated with the ground data, wherever available (e.g., soil moisture [51] discharge data [52], and the performance should be further analyzed statistically for the study region into consideration. Also, the applicability of the model as an auxiliary data source for GRACE-based water storage estimation can further be characterized either using more recent satellite datasets of soil moisture (e.g., SMAP; Soil Moisture Active Passive), land water storage (e.g., Swarm [53]), among others. Additionally, wherever available, the in-situ data records can also be used to further evaluate the model's performance to simulate the individual water storage components. Advancements towards hyper-resolution global water resource modeling and improved methods of satellite gravimetry will further enhance our understanding of the various regional and global hydrological systems.

4. Gravity Recovery and Climate Experiment (GRACE) data

The most recently released Level-06 (RL06M v02) monthly GRACE mascon (mass concentration) solutions from two processing centers, namely, the Jet Propulsion Laboratory and Centre for Space Research (JPL-M and CSR-M, respectively, thereafter) were used for characterizing the dynamics of land water storage (LWS_g) over the study region [54–57]. This newest data has been corrected in several aspects compared to the previous versions, such as representation on ellipsoidal Earth applied separately to land and ocean to minimize signal leakage, application of the Coastline Resolution Improvement filter leading to the reduced leakage errors across coastlines, the inclusion of the realistic geophysical information during the solution inversion to intrinsically remove correlated errors, among others. Additionally, unlike the conventional spherical harmonic approach, given their regularization process (and hence reduced systematic errors), mascons do not need any additional postprocessing in terms of signal restoration [58–60]. Data from April 2002 through December 2014 were used to minimize the uncertainties in GRACE estimates, especially at the seasonal time scales, which might have been induced due to the operational issues towards the end of the mission [61]. Since the ensemble mean of the two independent gravity products is found effective in reducing the uncertainty errors in the gravity fields (e.g., [62–64], an arithmetic average of LWS_g derived from the two mascon solutions was used for further analysis. The basin-wide LWS_g are presented in terms of the basin-wide equivalent water depth (mm) or equivalent water volume (km^3) anomalies relative to the long-term mean of 04/2002 to 12/2014. The missing values in the data series since early 2011 due to the active battery management were filled by the linear interpolation of the two bounding values [63,65].

5. Hodrick-Prescott (HP) filter

For a doubly infinite series, the cyclic component was estimated in the given data time series y_t by the high pass filter [66];

$$\tilde{c_t} = \tilde{H}(L) y_t \quad \text{(S1)}$$

where $\tilde{H}(L)$ is the weight function with L as the loss parameter. $\tilde{H}(L)$ is given by

$$\tilde{H}(L) = \frac{\lambda (1-L)^2 (1-L^{-1})^2}{1+\lambda (1-L)^2 (1-L^{-1})^2} = \frac{\lambda L^{-2}(1-L)^4}{1+\lambda L^{-2}(1-L)^4} \quad \text{(S2)}$$

where, λ (=1600, as most commonly used [67]) is the user-defined smoothing parameter. The trend component is then separated by the low pass filter;

$$T_t = \left(1 - \tilde{H}(L)\right) y_t = (1 + \lambda (1-L)^2 (1-L^{-1})^2)^{-1} y_t \quad \text{(S3)}$$

where T_t is the HP trend in the respective time series.

6. Water storage deficits, drought severity, and recovery time

Land water or groundwater storage deficits (LWSD or GWSD), i.e., deseasonalized LWS_m or GWS_m (monthly climatology removed from the original anomaly time series), quantify the instantaneous drought conditions in the land water or groundwater by the departures from the normal circumstances in the particular region but do not depict the severity during the whole period of the event. Moreover, LWSD/GWSD does not provide any information of the time elapsed before the water storage conditions return to normal, which is imperative for basin-scale water management and policymaking. Therefore, in addition to LWSD/GWSD analysis, we further calculated the event severity (Eq. S4 is the same as Eq. 3), which represents the cumulative water storage deficit (WSD) for a particular drought event (during the period of negative WSD) and thus highlights the overall water loss during the event. The product was used to evaluate the cumulative severity of the individual hydrological drought events [22];

$$S_t = \bar{M}_t * D_t \quad \text{(S4)}$$

where S_t is the event severity (mm months or km^3 month), $\bar{M}_t$ (mm or km^3) and D_t (months) are the average water deficit and duration since the onset of the deficit period, respectively. The subscript t signifies that all the parameters are a function of time. S_t characterizes the accumulated influence of deficiency associated with a particular drought event.

Further, we calculated the recovery time corresponding to monthly storage deficits (both LWSD and GWSD). First, we calculated the rate of change in the monthly water storage deficit as below:

$$\frac{d(WSD)}{dt} = \frac{WSD_i - WSD_{i-1}}{\Delta t} \text{ for } i = 1 \sim n \quad \text{(S5)}$$

where $\frac{d(WSD)}{dt}$ is the rate of change in LWSD or GWSD (evaluated only for the drought events), Δt is unity since the change was calculated during the consecutive months $i-1$ and i, and n is the length of LWS_m data record. For estimating the recovery time for each month's deficit, which is defined as the time to recover to the average storage conditions, the empirical cumulative distribution function (eCDF) of the $\frac{d(WSD)}{dt}$ series was calculated for three basins, all of which follow the normal distribution according to the Kolmogorov-Smirnov (K-S) test for the whole time series (see Fig. S1 below). The 95^{th} percentile (two-sigma) of the normally distributed eCDF represents the maximum positive rate of change of LWSD/GWSD, and hence the minimum recovery time was obtained by dividing the LWSD/GWSD for the particular month (in mm or km^3) with 2σ value of eCDF (in mm $month^{-1}$ or km^3 $month^{-1}$ corresponding to figures S1b and S1d, for GWSD and LWSD, respectively). Thus derived recovery time (in months) provides a physical time scale to get back to the normal storage conditions during each drought event.

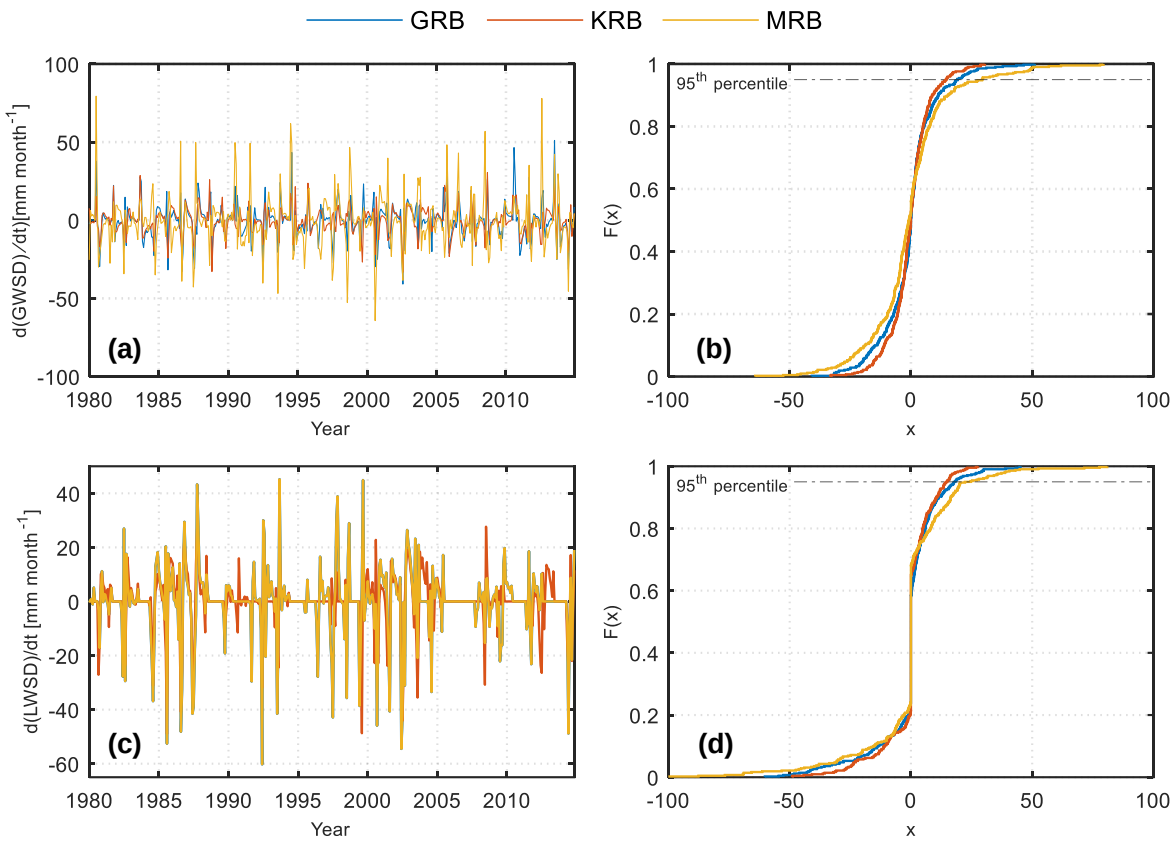

Figure S1. Recovery time calculation. Left: The time derivative of monthly WSD (GWSD and LWSD) considering both positive and negative deficits. Right: empirical cumulative distribution (eCDF) of d(WSD)/dt and 95th percentile used to determine the minimum time to recovery, all for 35 years.

7. Standardized indices

a. Self-calibrating Palmer Drought Severity Index (sc-PDSI)

The self-calibrating Palmer Drought Severity Index (sc-PDSI) was used for evaluating the long-term droughts in the basins and for quantifying their association with climate change. The sc-PDSI was evaluated using the regional level water balance incorporating four inputs, namely, precipitation, air temperature, latitude, and field capacity of the underlying soil, following the open access MATLAB tool developed by [68]. This method incorporates the two-bucket system-based water balance equation as below:

$$L_U = \frac{[(ET-P)-L_S]S_U}{FC} \quad \text{(S6)}$$

where L_U and L_S are the water loss from the underlying and surface layers, respectively, ET is the average potential evapotranspiration using the Thornthwaite and Hamon PET methods (applied for avoiding any bias associated with a particular method), P and S_U are the precipitation and the water amount in the underlying layer, FC is the field capacity of the combined soil layers. Monthly Z-values were calculated using the water balance output and the full record as the calibration period. This method is based on the assumptions and definitions by [69]. Firstly, a monthly water balance is calculated, followed by the calculation of the z-index and finally, the PDSI. Ls is the loss due to the evapotranspiration from the surface layer, which occurs when ET>P (evapotranspiration > precipitation) for a particular month and is assumed to be at a potential rate. S_U is the amount of water available in the underlying soil layer, which determines the water loss from the layer (L_U). FC, i.e., field capacity or the available moisture capacity, is the total moisture capacity of the system. All of these parameters were calculated by the MATLAB tool, details of which can be found in [68]. This method outperforms the traditional PDSI calculation methods in terms of sensitivity to the potential evapotranspiration (PET), computational simplicity, and transparency [68].

b. 12-month Standardized Precipitation Index (SPI12)

For the Standardized Precipitation Index, 12-months SPI (SPI12) was used for comparing the inter- and intra-basin drought conditions since shorter time SPIs are highly sensitive to the short-term precipitation fluctuations and do not reflect the multiyear droughts robustly [70]. SPI quantifies the standardized departure of precipitation from the long-term mean using the normal distribution (transformed from gamma distribution using equal probability function) [71]. Since the short time-scaled precipitation anomalies are reflected only in the soil moisture dynamics, SPI12 was used to effectively incorporate its reflection on the integrated land water storage dynamics on the basin scale.

Detailed reasoning of selecting SPI12 over other shorter time period SPI's is as below,

The 3-month (or shorter) SPIs reflect short- and medium-term moisture conditions and provide a seasonal precipitation estimation. These SPIs may lead to misinterpretation of the droughts when a temporary wet or dry period occurs [70]. Continuous and persistent drought monitoring is imperative to accurately determine when droughts begin and end. Large negative or positive in 3-month (or shorter) SPIs may be associated with precipitation totals that are not very different from the long-term

mean. This behavior becomes much more critical in the Peninsular Indian region, experiencing the high variability of the precipitation extremes due to the south Asia monsoon.

The 6-month SPI indicates seasonal to medium-term trends in precipitation and is still considered to be sensitive to the short-term extreme precipitation conditions. The 9-month SPI indicates inter-seasonal precipitation patterns over a medium timescale duration. Droughts usually take a season or more to develop [70], and hence may not be accurately represented by these short SPIs.

The 12-month SPI reflects long-term precipitation patterns and tends to gravitate toward zero unless a distinctive wet or dry trend is taking place. Also, the multiyear droughts resulting from the various water storage components (even including the groundwater storage) are evident in the 12-month SPI. Moreover, the PDSI is more closely related to the 12-month SPI than the short-term SPIs [70]. Since our focus is to determine the long-term droughts based on the total water storage and their comparison with the other indices, keeping the above points into consideration and similar to the previous studies (e.g., [58], we have selected the 12-month SPI.

c. Normalized land water storage index (WSDI)

First, water storage deficit (WSD) based drought indices for both LWS_m and LWS_g were calculated. The long-term mean of monthly LWS_m/LWS_g was calculated for each month by averaging the monthly values of the LWS_m/LWS_g anomaly. This climatology was then subtracted from the original time series of LWS_m/LWS_g anomaly to give the water storage deficit amount in a particular month as,

$$WSD_{j,k} = LWSA_{j,k} - \overline{LWSA_k} \quad \text{(S7)}$$

where WSD is the water storage deficit, subscripts j and k depict the year and month, respectively, $LWSA_{j,k}$ is the land water storage anomaly (based on LWS_m or LWS_g) for the j^{th} year and k^{th} month, $\overline{LWSA_k}$ represents the average monthly LWS_m anomaly over 35 years or LWS_g anomaly over 12 years. Monthly deficits (i.e., deseasonalized time series) in other modeled WS components, i.e., SMS_m and GWS_m, were also calculated using Eq. S7.

Since the water storage deficits represented as volumetric water storage may sometimes be ambiguous in interpretation since for a given deficit volume, a smaller area will have a higher intensity of the drought than the larger area. Therefore, to eliminate the effect of the geographical area on our analyses, the volumetric WSD was further calculated as basin-wide equivalent water depth. Also, for suitability of comparative assessment and inter-comparison among the other traditional indices, WSD was normalized to get the water storage deficit index (WSDI) following zero-mean normalization procedure [21];

$$WSDI_{j,k} = \frac{WSD_{j,k} - \mu}{\sigma} \quad \text{(S8)}$$

where $WSDI_{j,k}$ is the normalized water storage deficiency index (WSDI; $WSDI_m$ based on LWS_m and $WSDI_g$ based on LWS_g) for the j^{th} year and k^{th} month, μ and σ represent the mean and standard deviation of the time series of WSD, respectively.

d. In-situ groundwater level data

India's Central Ground Water Board (CGWB) has been maintaining and monitoring a dense network of operational groundwater wells (>15000 in total during 2014-our study duration, which is continually increasing) in India ([72–75]. The in-situ groundwater level is measured seasonally, i.e., four times a year during January (post-monsoon), May (pre-monsoon), August (monsoon-time), and November (post-monsoon) [72]. After screening the wells for temporal continuity (wells having two or more continuous gaps were precluded from the analysis) and applying the inter Interquartile range (IQR) filter (essentially for reducing outliers and partly the impact of confined aquifers) [76–78], data of 1080 wells distributed in the three study basins was further used (Figure 1, Table S1). These wells comprise about 32% of piezometers and 68% of the observation/monitoring wells, and the majority (~70%) of the wells are dug wells [74]. Most (~88%) of the wells in the study area are located in the unconfined shallow aquifer [73].

Further, for individual wells, the long-time (from May 2002 to Nov 2014) of the groundwater level is subtracted from the time series, and then the sign is reversed for depth conversion and multiplied with the S_y value to get the groundwater storage anomaly (GWSA) associated with the particular well. The individual GWSA calculated per well was further converted to the basin-wide GWSA time series using the simple Thiessen polygon method as below,

$$\mathrm{GWSA_t} = \frac{\sum_{i=1}^{n} \mathrm{A_i} * \mathrm{GWSA_i}}{\sum_{i=1}^{n} \mathrm{A_i}} \quad \text{(S9)}$$

where $\mathrm{GWSA_t}$ is the resulting basin-scale GWSA for month t, A_i is the area of Thiessen polygon corresponding to well i.

Most parts of central and southern India, consisting of our study basins, are composed of Pre-Cenozoic crystalline rocks, consolidated sedimentary formations, and multi-layered basalt flows of the Indian craton [73]. Moreover, since all three study basins possess a uniform hydrogeological setting (both GRB and KRB are primarily composed of jointed or fractured crystalline aquifer systems and MRB is composed of fractured crystalline or consolidated and permeable sedimentary aquifers) [79,80], similar to previous studies (e.g., [8,14], assumption of an average value of specific yields (S_y) was made for each basin (GRB: 0.023, KRB: 0.022, MRB: 0.039) [79]. Unlike the Indo-Gangetic Plain, consisting of the Indus and Ganges river basins, where the hydrogeology is predominantly unconsolidated sedimentary aquifers (sandy alluvium), and the maximum groundwater table depth is about 1.7 to 2.5 times higher than our study basins [72,79], the use of distributed specific yields is highly unlikely to improve the observed groundwater storage time series. To test this assertion, we compared our observed GWS with those from previous studies [18,79] using the unique value of S_y for individual well for a common period of May 2002 to November 2014. Both the time series agree well (Pearson correlation, r=0.97-0.99; Spearman's rho, ρ~0.98; p<0.001), and therefore we infer that the assumption uniform S_y value does not lead significant uncertainties in our results of long-term trends and/or subsequently derived normalized drought indices.

e. Groundwater Drought indices (GWDI)

Since the in-situ groundwater is available only four times a year and hence may not give a clear idea of the storage dynamics, we converted the in-situ data to the groundwater drought index. A statistical comparison of the three drought indices viz., GRACE based GWDI ($GWDI_g$), GWS_m based GWDI ($GWDI_m$), and observed GWDI ($GWDI_o$) (all calculated as per Eq. 4) was conducted to assess the potential of PCR-GLOBWB to quantify the groundwater drought conditions. Further details of the three types of GWDI used in our study are explained below,

GWS_m based GWDI ($GWDI_m$): GWDI based on the modeled groundwater (GWS_m) was calculated using the equation,

$$GWDI_{j,k} = \frac{GWSD_{j,k} - \mu}{\sigma} \quad \text{(S10)}$$

where $GWDI_{j,k}$ is the normalized index corresponding to GWS_m for the j^{th} year and k^{th} month, μ and σ represent the mean and standard deviation of the respective time series, respectively.

Obs-GWS (GWS_o) based GWDI ($GWDI_o$): GWDI based on the observed groundwater storage was calculated using the in-situ GWSA time series described in section 7d above and employing the Eq. S10 above.

GRACE-GWS based GWDI ($GWDI_g$): First, GRACE based GWS (GWS_g) was calculated using the regional water balance,

$$GWSA = LWSA - SWSA - SMSA \quad \text{(S11)}$$

where LWSA, SWSA, and SMSA are the anomalies of the GRACE-based land water storage (LWS_g), modeled surface water storage (SWS_m), and modeled soil moisture storage (SMS_m), respectively. All the water storage components were used as monthly time series. Due to the insignificant long-term trend in modeled surface water storage (SWS_m) and the absence of snowfall events in the study region, the surface water and snow water storage components are not explicitly shown in the relevant figures. Also, similar to the previous studies [8], due to the inability of GRACE satellites to detect the changes in biomass, this component was also excluded from Eq. S11. The GRACE-based GWDI was then calculated following Eq. S10.

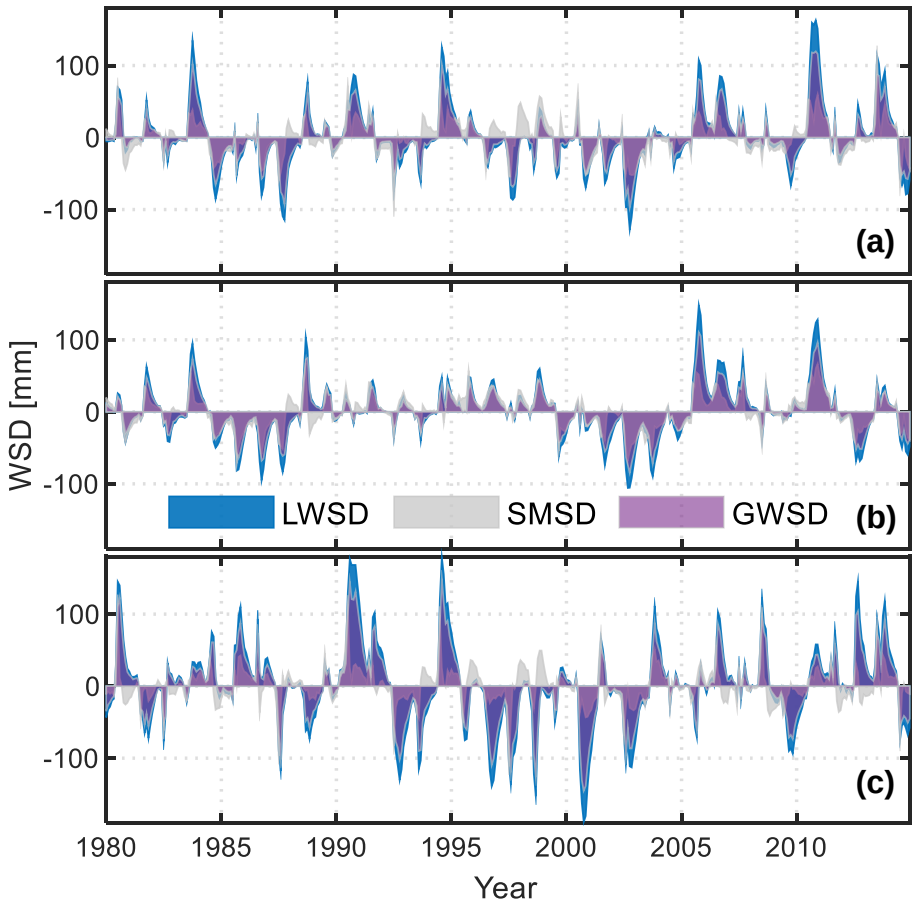

Figure S2. Monthly time series of water storage deficits (WSD). Water storage deficits (both depletion and recoveries, i.e., positive and negative storages) in various components (LWS_m, SMS_m and GWS_m) for GRB (a), KRB (b), and MRB (c). LWSD stands for land water storage deficit, and so on for SMSD and GWSD. This seasonal variability of the water storage deficits was calculated by removing the climatology of the respective component for 35 years from Jan 1980 until Dec 2014 (Eq. 2).

8. Impact of South Asia Monsoon

The climate of all three river basins is dominated by the South Asian summer monsoon, contributing about 80-85% of annual rainfall in the study region. Precipitation in the whole study region shows a seasonal variation due to this monsoon from July to October. The most pronounced fluctuations in the Mahanadi River Basin are followed by the Godavari and Krishna river basins. GWS anomalies attain a minimum value in May/June in all three basins, which is the end of the summer season and the monsoon's onset in the region. The importance of the South Asian summer monsoon in India can be understood by the fact that even minor spatiotemporal variabilities in its annual cycle have led to some severe drought conditions. These climatic variations subsequently derive the dynamics of the surface water storage (and groundwater withdrawal), which further propagate to soil moisture and groundwater storage, and eventually reflect in the land water storage.

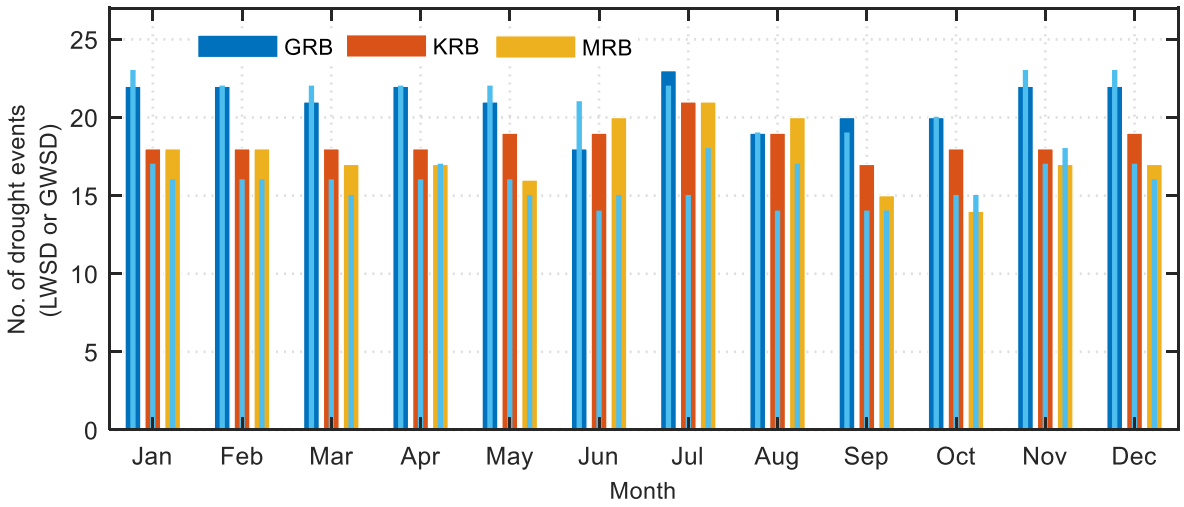

Figure S3. Intra-annual distribution of LWSD and GWSD. Intra-annual distribution (i.e., a monthly distribution) of land water storage deficits (LWSD) and groundwater storage deficits (GWSD) in the three river basins from Jan 1980 to Dec 2014. Colored and overlaid sky-blue bars represent the LWSD (based on LWS_m) and GWSD (based on GWS_m) respectively.

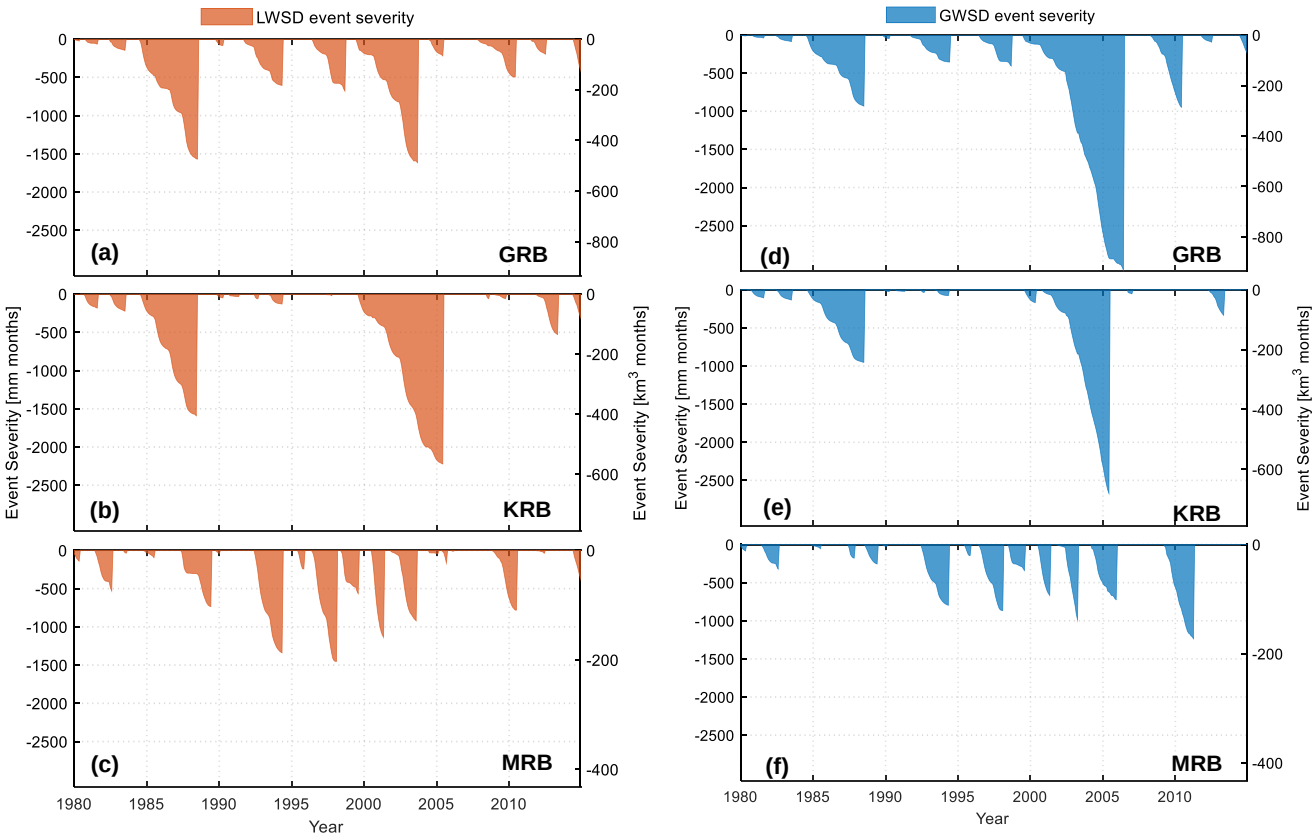

Figure S4. LWSD and GWSD events severity. **(a)-(c)** Severity (S_t) of the drought events identified based on the water storage deficits (WSD) derived from LWS_m (i.e., LWSD) for the (a) Godavari, (b) Krishna, and (c) Mahanadi river basins. **(d)-(f)** Severity (S_t) of the drought events identified based on the water storage deficits (WSD) derived from GWS_m (i.e., GWSD) for the (a) Godavari, (b) Krishna, and (c) Mahanadi river basins. Event Severity (S_t) (mm months or km^3 months) is equivalent to the cumulative LWS_m/GWS_m deficit during the given drought period.

Table S1. Intercomparison of various drought indices. Pearson correlation of the drought indices of the three study basins. Spearman's rho is also shown in parentheses.

	Godavari River Basin (GRB)			**Krishna River Basin (KRB)**			**Mahanadi River Basin (MRB)**		
Index	sc-PDSI	SPI12	$WSDI_m$	sc-PDSI	SPI12	$WSDI_m$	sc-PDSI	SPI12	$WSDI_m$
sc-PDSI	–			–			–		
SPI12	0.77 (0.79)	–		0.76 (0.77)	–		0.63 (0.59)	–	
$WSDI_m$	0.62 (0.58)	0.59 (0.56)	–	0.69 (0.67)	0.63 (0.60)	–	0.54 (0.49)	0.38 (0.30)	–

Table S2. Drought classification criteria. Drought categorization criteria of the drought events based on various drought indices.

Drought category	**Drought condition**	**SPI12**	**sc-PDSI**	**WSDI**
D0	No drought	$-0.5 < S$	$-1.0 < P$	$0 < W$
D1	Mild drought	$-1.0 < S \leq -0.5$	$-2.0 < P \leq -1.0$	$-1.0 < W \leq 0$
D2	Moderate drought	$-1.5 < S \leq -1.0$	$-3.0 < P \leq -2.0$	$-2.0 < W \leq -1.0$
D3	Severe drought	$-2.0 < S \leq -1.5$	$-4.0 < P \leq -3.0$	$-3.0 < W \leq -2.0$
D4	Extreme drought	$S \leq -2.0$	$P \leq -4.0$	$W \leq -3.0$

S, P, and W represent SPI12, sc-PDSI, and WSDI, respectively.

References

1. Dai, A. Drought under global warming: A review. *Wiley Interdiscip. Rev. Clim. Chang.* 2011.
2. Tripathi, P.; Rabara, R.C.; Shulaev, V.; Shen, Q.J.; Rushton, P.J. Understanding water-stress responses in soybean using hydroponics system—A systems biology perspective. *Front. Plant Sci.* **2015**, doi:10.3389/fpls.2015.01145.
3. Dai, A. Increasing drought under global warming in observations and models. *Nat. Clim. Chang.* **2013**, doi:10.1038/nclimate1633.
4. Famiglietti, J.S.; Rodell, M. Water in the balance. *Science (80-.).* 2013.
5. Taylor, R.G.; Scanlon, B.; Döll, P.; Rodell, M.; Van Beek, R.; Wada, Y.; Longuevergne, L.; Leblanc, M.; Famiglietti, J.S.; Edmunds, M.; et al. Ground water and climate change. *Nat. Clim. Chang.* 2013.
6. Sharma, A.; Goyal, M.K. Assessment of ecosystem resilience to hydroclimatic disturbances in India. *Glob. Chang. Biol.* **2018**, doi:10.1111/gcb.13874.
7. Sinha, D.; Syed, T.H.; Famiglietti, J.S.; Reager, J.T.; Thomas, R.C. Characterizing drought in India using GRACE observations of terrestrial water storage deficit. *J. Hydrometeorol.* **2017**, doi:10.1175/JHM-D-16-0047.1.
8. Rodell, M.; Velicogna, I.; Famiglietti, J.S. Satellite-based estimates of groundwater depletion in India. *Nature* **2009**, doi:10.1038/nature08238.
9. Kumar, R.; Singh, R.D.; Sharma, K.D. Water resources of India. *Curr. Sci.* **2005**, doi:10.1002/047147844x.wr243.
10. Mishra, A.K.; Singh, V.P.; Desai, V.R. Drought characterization: A probabilistic approach. *Stoch. Environ. Res. Risk Assess.* **2009**, doi:10.1007/s00477-007-0194-2.
11. Samra, J.S. Review and Analysis of Drought Monitoring, Declaration and Management in India Available online: https://www.preventionweb.net/files/1868_VL102135.pdf.
12. GoI *Ground Water Year Book India 2016-17. Central Ground Water Board, Ministry of Water Resources. Faridabad: Government of India.*; 2017;
13. Long, D.; Chen, X.; Scanlon, B.R.; Wada, Y.; Hong, Y.; Singh, V.P.; Chen, Y.; Wang, C.; Han, Z.; Yang, W. Have GRACE satellites overestimated groundwater depletion in the Northwest India Aquifer? *Sci. Rep.* **2016**, doi:10.1038/srep24398.
14. Panda, D.K.; Wahr, J. Spatiotemporal evolution of water storage changes in India from the updated GRACE-derived gravity records. *Water Resour. Res.* **2016**, doi:10.1002/2015WR017797.
15. Dasgupta, S.; Das, I.C.; Subramanian, S.K.; Dadhwal, V.K. Space-based gravity data analysis for groundwater storage estimation in the Gangetic plain, India. *Curr. Sci.* **2014**, doi:10.18520/cs/v107/i5/832-844.
16. Tiwari, V.M.; Wahr, J.; Swenson, S. Dwindling groundwater resources in northern India, from satellite gravity observations. *Geophys. Res. Lett.* **2009**, doi:10.1029/2009GL039401.
17. Chinnasamy, P.; Hubbart, J.A.; Agoramoorthy, G. Using remote sensing data to improve groundwater supply estimations in Gujarat, India. *Earth Interact.* **2013**, doi:10.1175/2012EI000456.1.

18. Abhishek; Kinouchi, T. Synergetic application of GRACE gravity data, global hydrological model, and in-situ observations to quantify water storage dynamics over Peninsular India during 2002–2017. *J. Hydrol.* **2021**, *596*, 126069, doi:https://doi.org/10.1016/j.jhydrol.2021.126069.

19. Satish Kumar, K.; Venkata Rathnam, E.; Sridhar, V. Tracking seasonal and monthly drought with GRACE-based terrestrial water storage assessments over major river basins in South India. *Sci. Total Environ.* **2020**, doi:10.1016/j.scitotenv.2020.142994.

20. Creutzfeldt, B.; Ferré, T.; Troch, P.; Merz, B.; Wziontek, H.; Güntner, A. Total water storage dynamics in response to climate variability and extremes: Inference from long-term terrestrial gravity measurement. *J. Geophys. Res. Atmos.* **2012**, doi:10.1029/2011JD016472.

21. Sun, Z.; Zhu, X.; Pan, Y.; Zhang, J.; Liu, X. Drought evaluation using the GRACE terrestrial water storage deficit over the Yangtze River Basin, China. *Sci. Total Environ.* **2018**, doi:10.1016/j.scitotenv.2018.03.292.

22. Thomas, A.C.; Reager, J.T.; Famiglietti, J.S.; Rodell, M. A GRACE-based water storage deficit approach for hydrological drought characterization. *Geophys. Res. Lett.* **2014**, doi:10.1002/2014GL059323.

23. Zargar, A.; Sadiq, R.; Naser, B.; Khan, F.I. A review of drought indices. *Environ. Rev.* 2011.

24. Bloomfield, J.P.; Marchant, B.P. Analysis of groundwater drought building on the standardised precipitation index approach. *Hydrol. Earth Syst. Sci.* **2013**, doi:10.5194/hess-17-4769-2013.

25. Wilhite, D.A.; Svoboda, M.D.; Hayes, M.J. Understanding the complex impacts of drought: A key to enhancing drought mitigation and preparedness. *Water Resour. Manag.* **2007**, doi:10.1007/s11269-006-9076-5.

26. Mishra, A.K.; Singh, V.P. A review of drought concepts. *J. Hydrol.* 2010.

27. Heim, R.R. A review of twentieth-century drought indices used in the United States. *Bull. Am. Meteorol. Soc.* 2002.

28. Niemeyer, S. New drought indices. *Options Méditerranéennes* **2008**, doi:10.1017/CBO9781107415324.004.

29. Cao, Y.; Nan, Z.; Cheng, G. GRACE gravity satellite observations of terrestrial water storage changes for drought characterization in the arid land of northwestern China. *Remote Sens.* **2015**, doi:10.3390/rs70101021.

30. Yi, H.; Wen, L. Satellite gravity measurement monitoring terrestrial water storage change and drought in the continental United States. *Sci. Rep.* **2016**, doi:10.1038/srep19909.

31. Yirdaw, S.Z.; Snelgrove, K.R.; Agboma, C.O. GRACE satellite observations of terrestrial moisture changes for drought characterization in the Canadian Prairie. *J. Hydrol.* **2008**, doi:10.1016/j.jhydrol.2008.04.004.

32. Wang, J.; Jiang, D.; Huang, Y.; Wang, H. Drought analysis of the Haihe river basin based on GRACE terrestrial water storage. *Sci. World J.* **2014**, doi:10.1155/2014/578372.

33. Sutanudjaja, E.H.; Van Beek, R.; Wanders, N.; Wada, Y.; Bosmans, J.H.C.; Drost, N.; Van Der Ent, R.J.; De Graaf, I.E.M.; Hoch, J.M.; De Jong, K.; et al. PCR-GLOBWB 2: A 5 arcmin global hydrological and water resources model. *Geosci. Model Dev.* **2018**, doi:10.5194/gmd-11-2429-2018.

34. Wada, Y.; Wisser, D.; Bierkens, M.F.P. Global modeling of withdrawal, allocation and

consumptive use of surface water and groundwater resources. *Earth Syst. Dyn.* **2014**, doi:10.5194/esd-5-15-2014.

35. Long, D.; Yang, Y.; Wada, Y.; Hong, Y.; Liang, W.; Chen, Y.; Yong, B.; Hou, A.; Wei, J.; Chen, L. Deriving scaling factors using a global hydrological model to restore GRACE total water storage changes for China's Yangtze River Basin. *Remote Sens. Environ.* **2015**, doi:10.1016/j.rse.2015.07.003.

36. Bosmans, J.H.C.; Van Beek, L.P.H.; Sutanudjaja, E.H.; Bierkens, M.F.P. Hydrological impacts of global land cover change and human water use. *Hydrol. Earth Syst. Sci.* **2017**, doi:10.5194/hess-21-5603-2017.

37. Weedon, G.P.; Balsamo, G.; Bellouin, N.; Gomes, S.; Best, M.J.; Viterbo, P. The WFDEI meteorological forcing data set: WATCH Forcing data methodology applied to ERA-Interim reanalysis data. *Water Resour. Res.* **2014**, doi:10.1002/2014WR015638.

38. Scanlon, B.R.; Zhang, Z.; Save, H.; Sun, A.Y.; Schmied, H.M.; Van Beek, L.P.H.; Wiese, D.N.; Wada, Y.; Long, D.; Reedy, R.C.; et al. Global models underestimate large decadal declining and rising water storage trends relative to GRACE satellite data. *Proc. Natl. Acad. Sci. U. S. A.* **2018**, doi:10.1073/pnas.1704665115.

39. Bhanja, S.N.; Mukherjee, A.; Rodell, M.; Wada, Y.; Chattopadhyay, S.; Velicogna, I.; Pangaluru, K.; Famiglietti, J.S. Groundwater rejuvenation in parts of India influenced by water-policy change implementation. *Sci. Rep.* **2017**, doi:10.1038/s41598-017-07058-2.

40. Yin, Z.; Xu, Y.; Zhu, X.; Zhao, J.; Yang, Y.; Li, J. Variations of groundwater storage in different basins of China over recent decades. *J. Hydrol.* **2021**, *598*, doi:10.1016/j.jhydrol.2021.126282.

41. Wang, Q.; Zheng, W.; Yin, W.; Kang, G.; Zhang, G.; Zhang, D. Improving the accuracy of water storage anomaly trends based on a new statistical correction hydrological model weighting method. *Remote Sens.* **2021**, *13*, doi:10.3390/rs13183583.

42. Abhishek; Kinouchi, T.; Sayama, T. A comprehensive assessment of water storage dynamics and hydroclimatic extremes in the Chao Phraya River Basin during 2002–2020. *J. Hydrol.* **2021**, *603*, doi:10.1016/j.jhydrol.2021.126868.

43. Felfelani, F.; Wada, Y.; Longuevergne, L.; Pokhrel, Y.N. Natural and human-induced terrestrial water storage change: A global analysis using hydrological models and GRACE. *J. Hydrol.* **2017**, *553*, doi:10.1016/j.jhydrol.2017.07.048.

44. Sperna Weiland, F.C.; Vrugt, J.A.; van Beek, R.L.P.H.; Weerts, A.H.; Bierkens, M.F.P. Significant uncertainty in global scale hydrological modeling from precipitation data errors. *J. Hydrol.* **2015**, doi:10.1016/j.jhydrol.2015.08.061.

45. Tangdamrongsub, N.; Steele-Dunne, S.C.; Gunter, B.C.; Ditmar, P.G.; Sutanudjaja, E.H.; Sun, Y.; Xia, T.; Wang, Z. Improving estimates of water resources in a semi-arid region by assimilating GRACE data into the PCR-GLOBWB hydrological model. *Hydrol. Earth Syst. Sci.* **2017**, doi:10.5194/hess-21-2053-2017.

46. Pai, D.S.; Sridhar, L.; Rajeevan, M.; Sreejith, O.P.; Satbhai, N.S.; Mukhopadhyay, B. Development of a new high spatial resolution (0.25° × 0.25°) long period (1901-2010) daily gridded rainfall data set over India and its comparison with existing data sets over the region. *Mausam* **2014**, *65*.

47. Döll, P.; Kaspar, F.; Lehner, B. A global hydrological model for deriving water availability indicators: Model tuning and validation. *J. Hydrol.* **2003**, *270*, doi:10.1016/S0022-1694(02)00283-

4.

48. Alcamo, J.; Döll, P.; Henrichs, T.; Kaspar, F.; Lehner, B.; Rösch, T.; Siebert, S. Development and testing of the WaterGAP 2 global model of water use and availability. *Hydrol. Sci. J.* **2003**, *48*, doi:10.1623/hysj.48.3.317.45290.

49. Döll, P.; Müller Schmied, H.; Schuh, C.; Portmann, F.T.; Eicker, A. Global-scale assessment of groundwater depletion and related groundwater abstractions: Combining hydrological modeling with information from well observations and GRACE satellites. *Water Resour. Res.* **2014**, doi:10.1002/2014WR015595.

50. Telteu, C.E.; Müller Schmied, H.; Thiery, W.; Leng, G.; Burek, P.; Liu, X.; Boulange, J.E.S.; Andersen, L.S.; Grillakis, M.; Gosling, S.N.; et al. Understanding each other's models An introduction and a standard representation of 16 global water models to support intercomparison, improvement, and communication. *Geosci. Model Dev.* 2021, *14*.

51. López, P.L.; Sutanudjaja, E.H.; Schellekens, J.; Sterk, G.; Bierkens, M.F.P. Calibration of a large-scale hydrological model using satellite-based soil moisture and evapotranspiration products. *Hydrol. Earth Syst. Sci.* **2017**, doi:10.5194/hess-21-3125-2017.

52. Sutanudjaja, E.H.; Van Beek, L.P.H.; De Jong, S.M.; Van Geer, F.C.; Bierkens, M.F.P. Calibrating a large-extent high-resolution coupled groundwater-land surface model using soil moisture and discharge data. *Water Resour. Res.* **2014**, doi:10.1002/2013WR013807.

53. Richter, H.M.P.; Lück, C.; Klos, A.; Sideris, M.G.; Rangelova, E.; Kusche, J. Reconstructing GRACE-type time-variable gravity from the Swarm satellites. *Sci. Rep.* **2021**, *11*, doi:10.1038/s41598-020-80752-w.

54. Save, H.; Bettadpur, S.; Tapley, B.D. High-resolution CSR GRACE RL05 mascons. *J. Geophys. Res. Solid Earth* **2016**, doi:10.1002/2016JB013007.

55. Save, H. CSR GRACE and GRACE-FO RL06 Mascon Solutions v02. **2020**, doi:doi: 10.15781/cgq9-nh24.

56. Wiese, D.N.; Yuan, D.-N.; Boening, C.; Landerer, F.W.; Watkins, M.M. JPL GRACE Mascon Ocean, Ice, and Hydrology Equivalent Water Height Release 06 Coastal Resolution Improvement (CRI) Filtered Version 1.0. Ver. 1.0. PO.DAAC, CA, USA.

57. Watkins, M.M.; Wiese, D.N.; Yuan, D.N.; Boening, C.; Landerer, F.W. Improved methods for observing Earth's time variable mass distribution with GRACE using spherical cap mascons. *J. Geophys. Res. Solid Earth* **2015**, doi:10.1002/2014JB011547.

58. Scanlon, B.R.; Zhang, Z.; Reedy, R.C.; Pool, D.R.; Save, H.; Long, D.; Chen, J.; Wolock, D.M.; Conway, B.D.; Winester, D. Hydrologic implications of GRACE satellite data in the Colorado River Basin. *Water Resour. Res.* **2015**, doi:10.1002/2015WR018090.

59. Li, B.; Rodell, M.; Kumar, S.; Beaudoing, H.K.; Getirana, A.; Zaitchik, B.F.; de Goncalves, L.G.; Cossetin, C.; Bhanja, S.; Mukherjee, A.; et al. Global GRACE Data Assimilation for Groundwater and Drought Monitoring: Advances and Challenges. *Water Resour. Res.* **2019**, doi:10.1029/2018WR024618.

60. Scanlon, B.R.; Zhang, Z.; Save, H.; Wiese, D.N.; Landerer, F.W.; Long, D.; Longuevergne, L.; Chen, J. Global evaluation of new GRACE mascon products for hydrologic applications. *Water Resour. Res.* **2016**, doi:10.1002/2016WR019494.

61. Chen, J.; Tapley, B.; Rodell, M.; Seo, K.W.; Wilson, C.; Scanlon, B.R.; Pokhrel, Y. Basin-Scale

River Runoff Estimation From GRACE Gravity Satellites, Climate Models, and In Situ Observations: A Case Study in the Amazon Basin. *Water Resour. Res.* **2020**, doi:10.1029/2020WR028032.

62. Sakumura, C. An ensemble solution for the Earth's time-varying gravitational field from the NASA/DLR GRACE mission, MSE Thesis, University of Texas at Austin. **2013**.

63. Xie, J.; Xu, Y.P.; Gao, C.; Xuan, W.; Bai, Z. Total Basin Discharge From GRACE and Water Balance Method for the Yarlung Tsangpo River Basin, Southwestern China. *J. Geophys. Res. Atmos.* **2019**, doi:10.1029/2018JD030025.

64. Sakumura, C.; Bettadpur, S.; Bruinsma, S. Ensemble prediction and intercomparison analysis of GRACE time-variable gravity field models. *Geophys. Res. Lett.* **2014**, doi:10.1002/2013GL058632.

65. Andrew, R.; Guan, H.; Batelaan, O. Estimation of GRACE water storage components by temporal decomposition. *J. Hydrol.* **2017**, doi:10.1016/j.jhydrol.2017.06.016.

66. Hodrick, R.J.; Prescott, E.C. Postwar U.S. Business Cycles: An Empirical Investigation. *J. Money, Credit Bank.* **1997**, doi:10.2307/2953682.

67. Ravn, M.O.; Uhlig, H. On adjusting the Hodrick-Prescott filter for the frequency of observations. *Rev. Econ. Stat.* 2002, *84*.

68. Jacobi, J.; Perrone, D.; Duncan, L.L.; Hornberger, G. A tool for calculating the palmer drought indices. *Water Resour. Res.* **2013**, doi:10.1002/wrcr.20342.

69. Alley, W.M. The Palmer Drought Severity Index: limitations and assumptions. *J. Clim. Appl. Meteorol.* **1984**, doi:10.1175/1520-0450(1984)023<1100:TPDSIL>2.0.CO;2.

70. WMO, W.M.O. Standardized Precipitation Index User Guide (M. Svoboda, M. Hayes and D. Wood). (WMO-No. 1090), Geneva.

71. Mckee, T.B.; Doesken, N.J.; Kleist, J. The relationship of drought frequency and duration to time scales.

72. Bhanja, S.N.; Rodell, M.; Li, B.; Saha, D.; Mukherjee, A. Spatio-temporal variability of groundwater storage in India. *J. Hydrol.* **2017**, *544*, doi:10.1016/j.jhydrol.2016.11.052.

73. CGWB *Central Ground Water Board (CGWB), G.o.I., Ministry of Water Resources. Ground Water Year Book – India 2013–14, 76pp*; 2014;

74. CGWB *Central Ground Water Board, CGWB. Ground Water Year Book—India 2016-17. G. o. I. Ministry of Water Resources, p. 90*; 2017;

75. India-WRIS River Basin Atlas of India, RRSC-West, NRSC, ISRO, Jodhpur, India.

76. Bhanja, S.N.; Mukherjee, A. In situ and satellite-based estimates of usable groundwater storage across India: Implications for drinking water supply and food security. *Adv. Water Resour.* **2019**, *126*, doi:10.1016/j.advwatres.2019.02.001.

77. Long, D.; Chen, X.; Scanlon, B.R.; Wada, Y.; Hong, Y.; Singh, V.P.; Chen, Y.; Wang, C.; Han, Z.; Yang, W. Have GRACE satellites overestimated groundwater depletion in the Northwest India Aquifer? *Sci. Rep.* **2016**, doi:10.1038/srep24398.

78. Davis, J.C. *Statistics and Data Analysis in Geology. (3rd edition), Wiley, New York*; 2002;

79. Bhanja, S.N.; Mukherjee, A.; Saha, D.; Velicogna, I.; Famiglietti, J.S. Validation of GRACE based groundwater storage anomaly using in-situ groundwater level measurements in India. *J. Hydrol.* **2016**, *543*, doi:10.1016/j.jhydrol.2016.10.042.

80. Dhiman, S.. *Aquifer systems of India. Ministry of Water Resources, Government of India*; 2012;